Available online at www.sciencedirect.com
SCIENCE DIRECT
Cement and Concrete Research 36 (2006) 346 – 357
Cement and Concrete Research

X-ray microtomography: Application to microstructure analysis of a cementitious material during leaching process

Nicolas Burlion[a,*], Dominique Bernard[b], Da Chen[a]

[a]Laboratory of Mechanics of Lille, UMR CNRS 8107, Polytech'Lille, Dpt GTGC, Cité Scientifique, 59650 Villeneuve d'Ascq, France
[b]ICMCB, UPR CNRS 9048, 87 Av. du Dr A. Schweitzer, 33608 Pessac, France

Received 5 April 2004; accepted 20 April 2005

Abstract

Leaching of cementitious materials leads to an increase in porosity, which has important consequences on transport and mechanical properties. The present study outlines the characterization of microstructural evolution in a mortar subjected to a chemical attack, by means of a powerful non-intrusive experimental method, namely synchrotron X-ray computed microtomography. This innovative method is used to measure the variation of porosity in a leached mortar. Having described the effects of leaching in mortar (influences on microstructure and on mechanical properties), we present the accelerated leaching process and the microtomographic analysis that have been used to monitor it. We then investigate the capacity of this method to quantify the evolution of porosity during the leaching process. The method is validated by comparison of the results obtained with data available in the literature.

Keywords: Leaching; X-ray absorption; Synchrotron X-ray microtomography; Mortar; Porosity evolution

1. Introduction

Mortars and concretes are non-homogeneous materials and their macroscopic physical properties depend on their local characteristics (physical properties of elementary components, micro-geometry, transport properties at a micro-level, etc...). For instance, porosity and permeability of concrete are intimately related to the microstructure. Thus it is of importance to link the local and the macroscopic scale in order to study and model the mechanical behaviour and the transport properties of cementitious materials. This requires the knowledge of the 3D micro-geometry.

Characterization of concrete or mortar microstructure, and its evolution, often raises problems: very small observation scales, interference of measurement with the material (thin section obtained by mechanical abrasion, scanning electron microscope analysis made under vacuum after material desiccation, etc...). In order to avoid these problems, various innovative techniques are in development as, for example, acoustic emission analysis, infrared thermography or X-ray computed microtomography (XCMT).

Synchrotron XCMT finds applications in the study of sample microstructure without damaging it (biological samples, geological or industrial materials) [1–3]. The principle, similar to the medical scanner, consists of acquiring digital images of the material's X-ray absorption. This acquisition is undertaken at various angles: a three-dimensional image is then obtained by numerical reconstruction from the set of 2D-images. This technique has already been used for cementitious materials, particularly mortars: to measure internal crack growth in small specimens under uniaxial compressive loading [4,5]; to quantify damage parameters of asphalt concrete specimens [6]; to evaluate sulphate attack effects on cement paste [7] and mortar [8]; to observe water evaporation with respect to time during drying [9,10]; to characterize the early hydration of calcium aluminate's cement [11]; or to validate numerical

* Corresponding author.
E-mail address: Nicolas.Burlion@polytech-lille.fr (N. Burlion).

0008-8846/$ - see front matter © 2005 Elsevier Ltd. All rights reserved.
doi:10.1016/j.cemconres.2005.04.008

simulations on mathematical analysis of concrete aggregate shapes [12] and on evolution of microstructure and transport properties of porous bricks [13]. The objective of the present study is to evaluate the increase in porosity induced by leaching of mortar by using synchrotron XCMT.

Concrete leaching is often the results of a fluid attack (pure water or water with very low pH compared to that of the pore fluid), and leads to the hydrolysis of cement paste hydrates [14–22]. This hydrolysis, which develops from the surface by diffusion of the aggressive agents through the material and diffusion of the dissolved products to the exterior, leads to an important increase in the cement paste porosity. As a consequence, liquid and gas transport properties are increased and the mechanical strength decreases [17,19–27]. Classical experimental methods used to study leaching effects [19,21,22,24–27] are often conducted by uncoupling the leaching process and other tests: for example, mechanical tests are usually performed after complete leaching. Furthermore, it remains very difficult to measure the evolution of porosity due to the leaching process, as numerous interactions occur between the experimental method and the leached material. One of the objectives of the present study is to obtain, with minimum interaction between the measurement and the degradation process, quantitative data about the effects of leaching on mortars. These unaffected data will then provide valuable validation of existing models [21–23,28–31] that predict loss of density of cement paste, evolution of porosity, or creation of porosity around aggregates.

Using synchrotron XCMT as a non-destructive characterisation method and performing the accelerated leaching with an ammonium nitrate solution, it is possible to carry out the microtomographic analysis on the same specimen during the leaching process. The evolution of the cement paste linear attenuation coefficient, the degradation kinetics, the leaching front position and the porosity increase can be determined without interfering with the material.

This paper is composed of three parts: first, we briefly describe mortar degradation mechanism caused by an aggressive solution, showing the importance of porosity increase and its mechanical consequences. In the second part, the chosen leaching process and the principles of synchrotron X-ray computed microtomography (XCMT) are clearly described. In the third part, the results obtained are depicted, demonstrating the capacity of the method to quantify the evolution of porosity and movement of the degradation front during leaching. Potential contributions of X-ray microtomography to a durability analysis of cementitious materials are emphasized.

2. Influences of porosity evolution due to leaching of cement paste

Calcium leaching is a coupled diffusion–dissolution process involving dissolution fronts that propagate through the sample. Under the influence of an aggressive solution (deionised water or ammonium nitrate solution), hydrolysis phenomena develop from the surface by diffusion of aggressive spices into the material and of dissolved products to outside, allowing the development of the leaching process by a front of dissolution/precipitation. With a decrease in pH of the pore solution, the first hydrate likely to be leached is the calcium hydroxide, also known as Portlandite. After complete dissolution of Portlandite, the calcium-silicates hydrates (C-S-H) are then decalcified [14,15]. Portlandite dissolution is associated with an important increase in capillary porosity, while the decalcification of C-S-H porosity results in only slight changes. Leaching kinetics is related to the material transfer properties: the lower the porosity, and the lower the degree of interconnection between pores, the lower will be the penetration of the aggressive solution.

Furthermore, there are some important differences between the bulk of the hydrated cement paste and the interface with aggregate (the so called interfacial transition zone—ITZ) in terms of porosity, hydration, and chemical composition. It can be assumed, in case of leaching, that the particular properties of this zone could contribute to an increase in mortar sensitivity compared to cement paste. Bourdette [16] estimated the role of aggregates in leaching a mortar, and identified only a weak influence of the ITZ. The chemical mechanisms are similar to those described by Adenot [14], as far as hydrated cement is the only reactive constituent. These results were confirmed by Carde and François [17,22]. An explanation of it could be the physical equivalence, in terms of porosity and transport properties, between the leached cement paste and this interfacial zone. On the other hand, the ITZ mechanical effect, in term of brittleness around aggregates during the leaching process, was demonstrated by Carde and François [17,22], which is in part due to the high Portlandite concentration within the ITZ.

2.1. Evolution of porosity

The main consequence of dissolution is a strong increase in material porosity [18,23], which amplifies the accessibility of external solutions to sound material and thus may amplify degradation phenomena. This porosity increase induced by leaching, reported in various works, is due to the loss of calcium: dissolution of Portlandite leads to a porosity growth corresponding to the initial volume of this constituent. Decalcification of C-S-H induces hydrate reorganization and modifies little their physical properties. Tognazzi [19] showed that the calcium decrease in the solid phase corresponds to the increase in total porosity of samples (cement paste and mortars with CPA-CEM I). This additional porosity is of comparable size to capillary porosity. C-S-H decalcification, which occurs after the Portlandite dissolution, only results in a small porosity modification compared to the variation caused by the Portlandite dissolution. Such results had also been observed by Revertegat et al. [20] or Gérard [21].

2.2. Calcium leaching and evolution of mechanical properties

Changes in mechanical properties of cementitious materials during leaching have been widely studied [17,21,22,24–26,28]. Compounds containing calcium are the main constituents of the cement paste and they provide most of the mechanical cohesion of this material. Carde and Carde et al. [22,31] attribute about 70% of the uniaxial compression strength to hydrated cement compounds containing calcium. For example, the loss of strength with leaching of a cement paste, with silica fume addition, is smaller as the pozzolanic reaction increases the development of C-S-H and reduces the Portlandite content [22,31]. C-S-H decalcification occurs much less readily than the dissolution of the Portlandite: the consequences in term of mechanical behaviour (strength in particular) are thus less. From microhardness tests on leached cement paste, Gérard [21] has proposed a relation between the elastic modulus and the loss in calcium: two important stages are detected. The first results from the dissolution of Portlandite, the second from of the decalcification of the last C-S-H compounds. Between these two stages, there is little variation in elastic modulus and the impact of C-S-H decalcification on mechanical properties is reported to be minor. These results were confirmed by other microhardness tests on leached cement paste, where the hardness is related to the material strength [32].

Furthermore, Carde [22] has shown a strong correlation between the porosity content and the uniaxial compression strength of the material. Measurements were performed on materials with different initial porosity: the porosity variations were obtained by using different formulations of cement paste or by leaching. A compression strength decrease is observed whatever the origin of the porosity increase is. From a mechanical modelling point of view, several approaches were successfully followed to describe the mechanical behaviour of a leached cement: use of a damage model [21,29–31] or an elasto-plastic model [24,28]. In both cases, the material behaviour is correctly reproduced and the porosity increase is usually taken as a major parameter. The experimental evaluation of this parameter is then essential in the description and the modelling of the evolution of the mechanical properties of cementitious materials subjected to leaching.

3. Experimental methods

3.1. X-ray microtomography used for leaching analysis

High resolution microtomographic acquisition was performed on the ID19 beam line of the European Synchrotron Radiation Facility (ESRF, Grenoble, France). In our case a monochromatic beam with energy of 27 keV was used: this was obtained by placing a monochromator composed of two vertical silicon single crystals into the polychromatic X-ray beam produced by the undulator of ID19.

The mortar sample was mounted on a rotating table and the acquisition consisted of the recording of 900 two-dimensional (2D) radiographs at equally spaced angles between 0° and 180° (Fig. 1). A scintillator placed behind the sample converts X-rays to visible light. Contrast obtained on the 2D projections results from the difference in X-ray absorption by the phases/features encountered by X-rays in the specimen (see Section 3.2). A mirror and the optical set-up selected for the experiment directed the light to the detector. The FRELON CCD camera, developed at ESRF, comprises 2048×2048 pixels. Depending on the characteristics of the optical set-up, a pixel of the CCD camera will correspond to a physical pixel on the sample having a size in the range of 40×40 and 0.3×0.3 μm^2. An initial set-up was selected to provide a pixel size of 4.9×4.9 μm^2 (in order to have a representative mortar specimen) but this was later changed to 7.46×7.46 μm^2, in order to improve contrast. The 2D radiographs were then exploited to reconstruct the volume of the samples using a conventional filtered backprojection algorithm [1–3].

At a given energy, absorption of X-rays is function of several physical parameters, mainly the local density and the atomic number of the material being traversed (see Section 3.2). In a porous material, if all the components of the solid phase have about the same X-ray absorption, the 3D-image of the absorption can be transformed into a 3D-image of the porosity. The use of microtomography in material science thus requires that the studied material presents differences of internal absorption, which can be measured within the studied volume elements (voxel). This technique is thus well adapted to multi-component materials, to porous materials, or to materials that evolve or mature (cement maturation or glass sintering [33]), or degrade (leaching, sulfate attack, mechanical compression).

With an X-ray source such as the ESRF, the resolution is limited by the digital sensor. In classical tomography, samples must have a maximal lateral dimension such that all the projections match the field of view of the digital camera. This constraint provides a means of calculating the maximal dimension (diameter for circular samples, etc...) as regards to the selected pixel size and resolution.

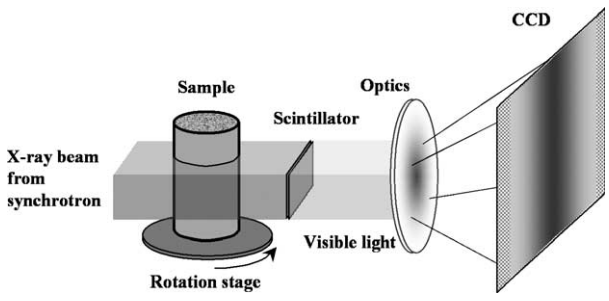

Fig. 1. Sketch of the experimental setup for microtomography mapping.

3.2. Principles of synchrotron XCMT

When a homogeneous material of linear attenuation coefficient μ is illuminated by a narrow beam of monochromatic photons of energy E, the ratio between N_0, the number of incident monochromatic photons, and N, the number of photons transmitted through a material thickness L is given by the Beer–Lambert law [2]:

$$N = N_0 \cdot e^{[-\mu \cdot L]}. \quad (1)$$

In the case of a heterogeneous material, it is necessary to interchange μL with the integral of μ along the photons path. The number of transmitted photon N' is then:

$$N' = N_0 e^{\left(-\int_{\text{path}} \mu(l)dl\right)}. \quad (2)$$

Measuring N_0 and N' allows the calculation of the integral of μ along this path line:

$$\ln \frac{N_0}{N'} = \int_{\text{path}} \mu(l)dl. \quad (3)$$

Let us now consider an heterogeneous object characterized by its 3D-mapping $\mu(x,y,z)$. We place it (Fig. 1) on a rotating table (rotation axis corresponding to z) in the X-ray beam (direction v) and ahead of the 2D detector (plane (u,z), with the axis u perpendicular to v). The synchrotron beam being parallel, each section perpendicular to the z-axis can be treated individually. Then, for an angular position θ of the rotation table (and of the object), at each point u on the detector, N' can be measured and Eq. (4) can be used to calculate the projection P:

$$P(\theta) = \{P(u,\theta);\ u = \pm r\} = \left\{\ln\left(\frac{N_0(u)}{N'(u)}\right) = \int_{\text{Ray } u} \mu(v)dv;\ u = \pm r\right\} \quad (4)$$

where $(-r)$ and $(+r)$ represent the extreme values of u on the detector, and Ray u the line parallel to v hitting the detector at u. The set of projections $P(\theta)$, for θ varying between 0° and 180°, is the Radon transform of $\mu(x,y)$. In 1917, Radon proved mathematically that it is possible to find an inverse to this transform and thus it is possible to reconstruct the 3D-map of μ from a set of projections.

The general principle of using the calculated 3D-map of the linear attenuation coefficient μ [cm^{-1}] is based on the fact that, for a pure material, the mass attenuation coefficient μ/ρ is correlated to the photon energy E and to the atomic number Z (for further details on the principle, see in general Ref. [2]). Below 200 keV, the following relation can be used:

$$\frac{\mu}{\rho} = K\frac{Z^4}{E^3} \quad (5)$$

where ρ is the material density [g/cm^3] and K a constant. Eq. (5) implies that at a given energy E, the linear attenuation coefficient μ is proportional to ρ and Z^4.

The mass attenuation coefficient μ/ρ of an heterogeneous material containing i elements (mass concentration w_i with specific mass attenuation coefficient $(\mu/\rho)_i$) is obtained with the following relation:

$$\frac{\mu}{\rho} = \sum w_i(\mu/\rho)_i. \quad (6)$$

3.3. Material choice and specimens design

The size of the sample was imposed by the microtomographic analysis. The maximum size was 2048×4.9 μm (about 10 mm). Cylindrical cores of 8 mm diameter were obtained from 37 mm diameter cylinders (Fig. 2). Their lengths varied between 20 and 30 mm.

To perform this study, a standard mortar (see Table 1) was made with standard sand (European standards), of a maximal grain size of 2 mm. Such mortar has the advantage of being reproducible by other laboratories without major difficulties. Furthermore, a sample of 8 mm diameter and 20 mm long can be considered as a representative volume of the material.

Samples—37 mm diameter—were cored and cut from a beam which had been cured in water at 20 °C for 6 months. After this curing, the effects of thermal and endogenous shrinkage will be negligible, while high maturity of the mortar was achieved. Desiccation of the samples, prior to microtomographic analysis and leaching, was avoided in order to avoid any risk of microcracking induced by drying, which would modify the kinetics of leaching due to the increase in the transport properties [34].

3.4. Accelerated leaching process

The objective of experiments is to analyse different leaching states of the mortar. This is achieved by an accelerated test which is able to reproduce a material response that characterizes the long-term behaviour of cementitious materials. The degradation process chosen

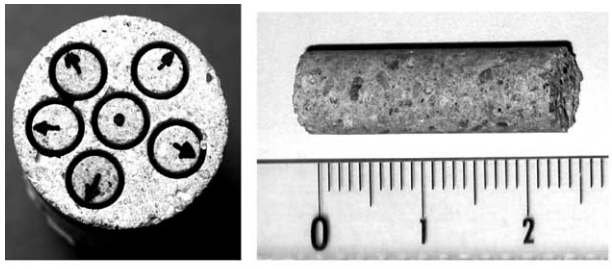

Fig. 2. Mortar specimen design: (a) initial ϕ37 mm mortar cylinder; (b) the ϕ8 mm used specimen.

Table 1
Composition of the used standard mortar

Components	Quantity
Standard sand 0/2 mm (EN 196-1[a])	1350 g
Cement CEM II/B 32,5 R[a]	450 g
Water	225 g
Water/cement ratio	0.5

[a]According to the European standards.

for this experimental study has to fulfil the following requirements: the material degradation must be achieved in, at most, 4 days, because of time assigned for the microtomographic analysis. Considering the geometry of the specimens, an accelerated test with ammonium nitrate solution was chosen.

The dissolution fronts are due to locally quasi-instantaneous dissolution. The time scale of the leaching process is governed by diffusion properties. Small sample sizes and high calcium efflux lead to a rapid leaching process [24]. Calcium efflux can be artificially accelerated by increasing the calcium solubility, close to the dissolution front, by using an ammonium nitrate solution (NH_4NO_3—480 g/kg_{H2O}). It has been shown that such a leaching process has very high kinetics (about 300 times the kinetics of leaching by deionised water [24,27]) and that the ammonium nitrate-based calcium leaching leads to the same mineral end products in the cementitious material [22].

After an initial image acquisition on the un-leached sample, the specimen was immersed for 24 h into the ammonium nitrate solution. This solution was regularly stirred during the leaching period (61 h). A second acquisition was made, and the sample was returned to the leaching solution. Two further acquisitions were performed after 48 and 61 h of leaching. The experimental advantage is that it is possible to directly compare data obtained with the same sample. This allows us to avoid a necessary statistical analysis by working on cementitious materials.

4. Results and discussions

4.1. Absorption variations of the 3 principal material phases with the leaching

After 3D-reconstruction by filtered backprojection, 3D-maps are obtained of the sample's X-ray linear attenuation coefficient μ at the four stages of leaching. Any cross section through the sample can be visualised. To analyse X-ray absorption variations in the cement, in the initial porosity and in the aggregates during the mortar leaching, we have chosen to firstly analyse a domain close to the surface of the sample, in order to compare the evolutions of absorption coefficient μ for each material phase during the complete leaching process. Fig. 3 shows the variation in the absorption coefficient μ for these three phases with respect to the leaching time: the aggregate absorption coefficient does not vary during the leaching process, as it does not react with the ammonium nitrate solution. The standard sand used (European standard EN 196-1) consists mainly of silica, and was chosen to not interfere with the cement leaching. Obviously, the leaching front seems not to be influenced by the local aggregate density (see Figs. 5-7), because the leaching process is essentially a diffusive phenomenon.

The absorption coefficient values (μ) in the cement paste rapidly decrease for the first 24 h, more slowly between 24 and 48 h of leaching, and finally become almost constant after 48 h. Note that the chosen analysis point is close to the surface sample. In this chosen degradation zone, it is possible to deduce that the decalcification of Portlandite crystals (CH) plays an essential role in the decrease of the μ-values for the first 24 h of leaching. Almost all Portlandite crystals react with the ammonium nitrate solution, and only a small amount of C-S-H is involved in the reactions (for the considered leaching time). Between 24 and 48 h of leaching, the decrease of the μ-value is smaller because C-S-H decalcification is more difficult than for Portlandite dissolution. After 48 h, the Portlandite is completely leached and the decalcification of C-S-H increases.

Finally, the measured absorption coefficient in the porosity varies little for 24 h of leaching, and then slowly decreases afterwards. To explain this variation, we must take into account the fact that the μ-value, estimated at each voxel, is a combination of the μ-values of all the

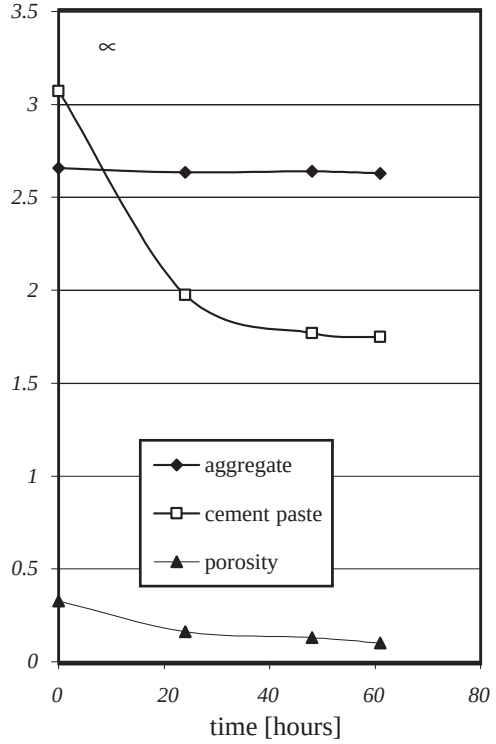

Fig. 3. Variation of absorption coefficient μ as a function of leaching time, for the different material phases.

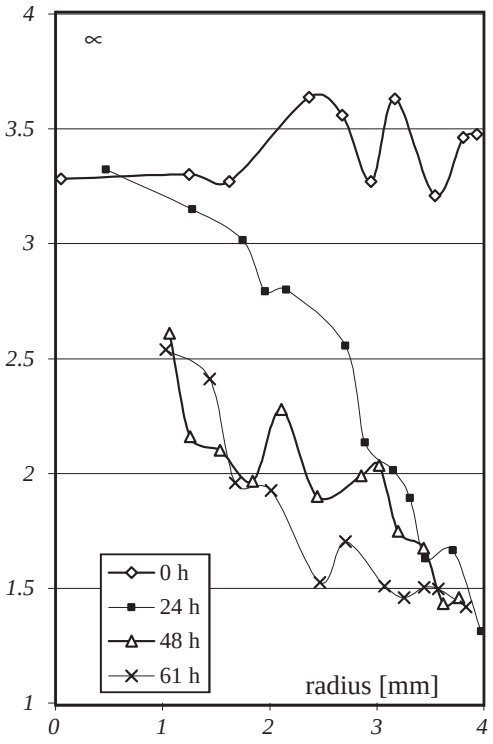

Fig. 4. Variations of absorption coefficient μ in the cement paste during the leaching.

components present in the voxel during the measurement (Eq. (6)), this is named as the "partial volume effect". This last result is much more affected by the "partial volume effect" than the two others are. Indeed, for the aggregates or the cement paste we selected small identical volumes (about 10 voxels) in each phase at each time; for porosity we selected a small pore. Some of the voxels considered for computation were partly filled with cement paste and the global variation takes into account the variation of μ for this phase. Selecting a zone with a large pore would have

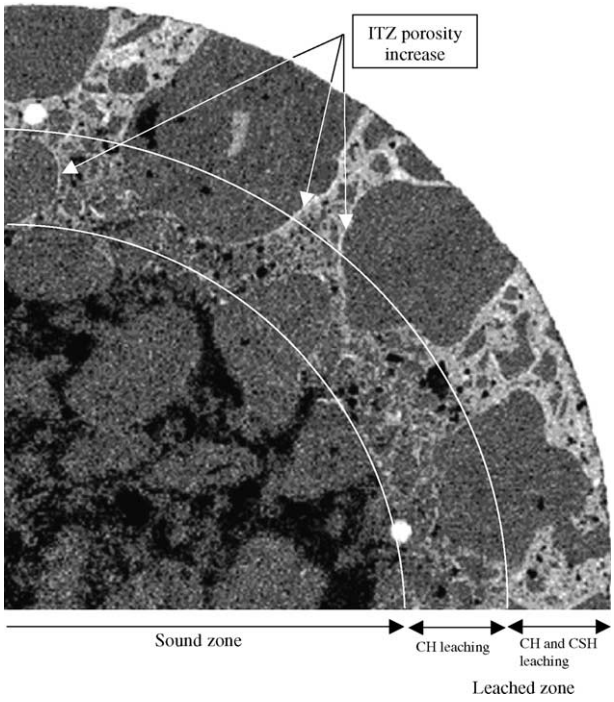

Fig. 6. Cross-section perpendicular to the sample axis after 24 h of leaching—identification of leached zones.

produced a better stability for the μ-value in porosity, but a stronger perturbation of the global behaviour.

4.2. Evolution of mortar porosity with leaching

4.2.1. Variation of absorption coefficient during the leaching test

To determine the degradation evolution inside the sample, we have measured the linear attenuation coefficient μ of the cement paste for various locations in the sample (at the same radius) and for the 4 acquisition times (0, 24, 48 and 61 h of leaching). Considering the symmetry, only half

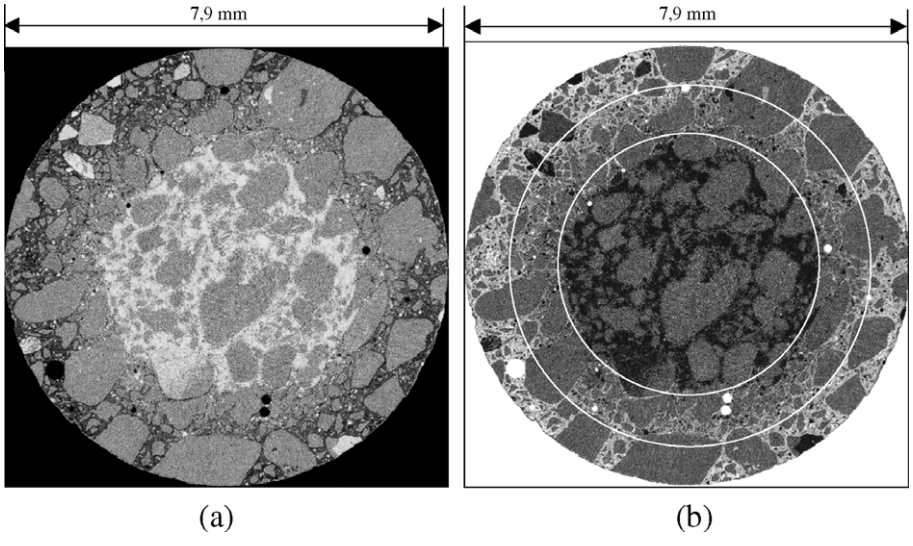

Fig. 5. Cross-sections perpendicular to the sample axis of the sample after 24 h of leaching (a) initial 2D-image; (b) negative view of the previous image.

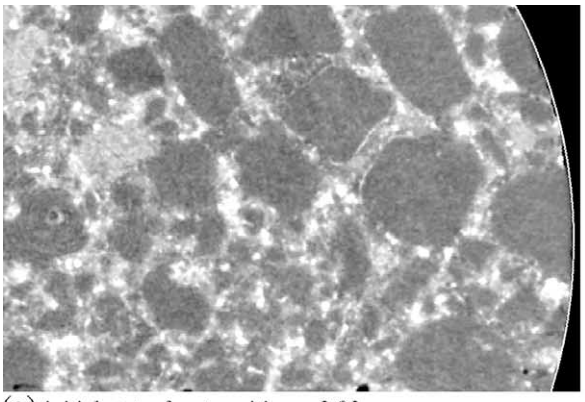

(a) initial state, front position = 3.93 mm

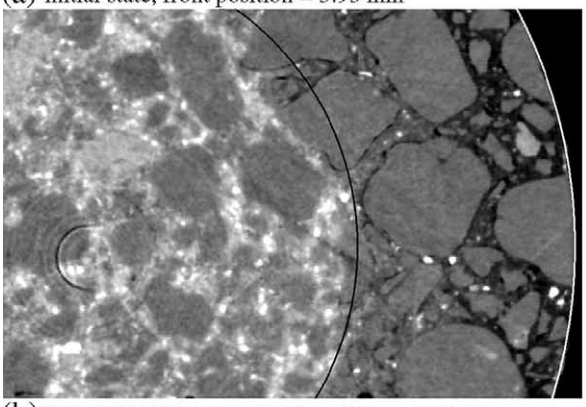

(b) 24 hours of leaching, front position = 2.25 mm

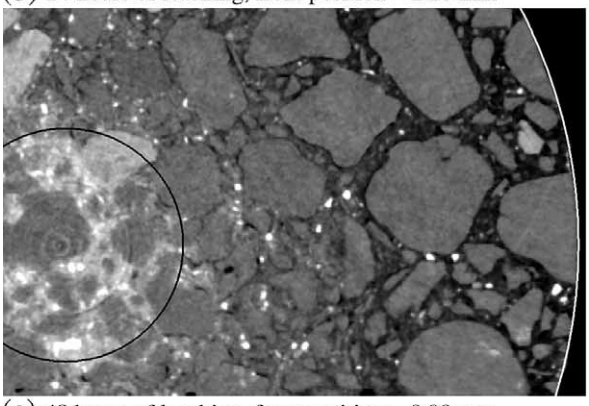

(c) 48 hours of leaching, front position = 0.90 mm

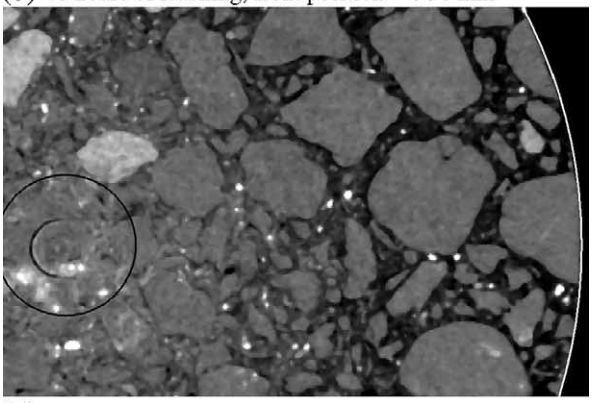

(d) 61 hours of leaching, front position = 0.58 mm

Fig. 7. Leaching front evolution: cross-sections of the sample at different leaching time.

a section is considered. Fig. 4 depicts variations of the absorption coefficient μ of the cement paste, according to the specimen radius, corresponding to the distance between the sample centre and the measured position. These results show:

- Before leaching, the absorption coefficient profile is relatively homogeneous around a mean value. The observed scattering results from cement paste components which are not uniform, in particular the local degree of hydration varies from one point to another. For the qualitative and quantitative analysis, we may suppose that the initial absorption coefficient of the cement paste corresponds to an average value, here 3.41, considering the maturity of mortar is very high.
- After 24-h leaching, 2 main zones appear: for a radius between 0 and 1.5 mm, values of the absorption coefficient μ do not vary, corresponding to the sound central zone. This is confirmed in Fig. 5a, a digital image of the sample cross section after 24 h-leaching. In this figure, it is possible to clearly distinguish aggregates, sound cement paste (in light grey), leached cement paste (darker grey) and macroporosity (dark circular zones). It still seems very difficult to distinguish the microporosity, because of the limited resolution. In Fig. 5b, the negative image of the previous one is shown: different domains can be identified. Black corresponds to the sound material; the dark grey region corresponds to the progressive dissolution of Portlandite and the domain where cement paste colour is light grey, in which Portlandite may be completely dissolved and where C-S-H decalcification has begun. These 3 domains are more clearly shown on Fig. 6. This picture also shows the influence of the interfacial transition zone around the aggregates: due to the particular chemical composition of

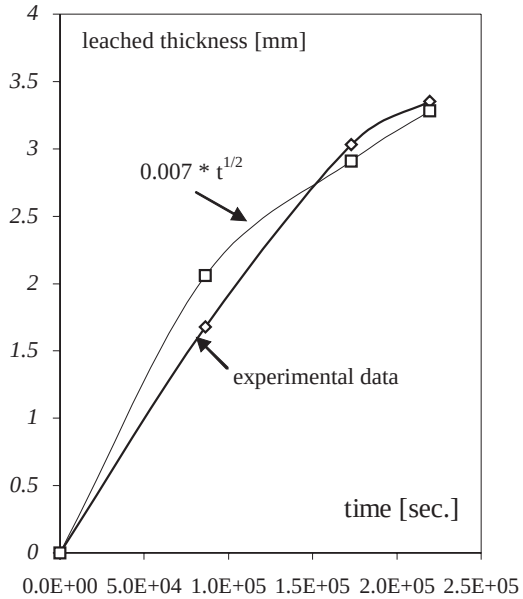

Fig. 8. Variation of leached thickness versus time.

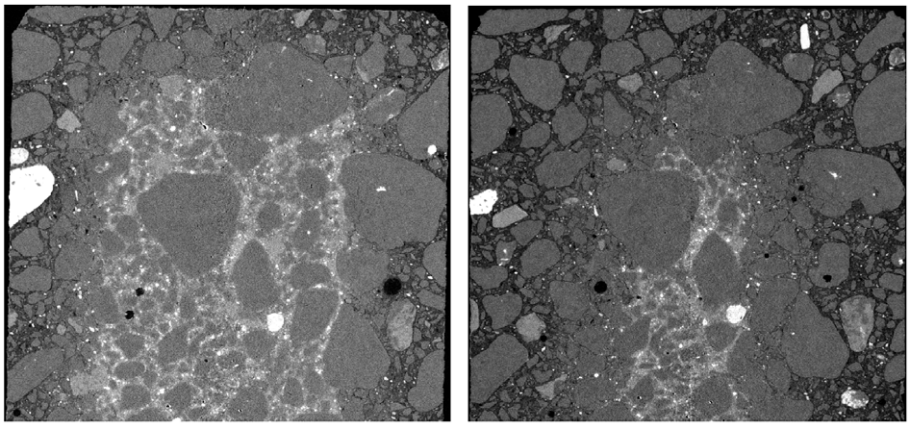

Fig. 9. Images at the different stages of leaching of sections parallel to the sample axis and approximately at the same position—evolution of the vertical leached front in 2D.

this interface, the leaching effect is more pronounced. For radii greater than 2 mm, the μ-values gradually decrease; corresponding to the dark grey zone on Fig. 6. For radii greater than 3 mm, the μ-values vary rapidly (light grey zone in Fig. 6). This phenomenon illustrates that Portlandite dissolution is uniform in the degraded zone, and that the progressive C-S-H decalcification concerns the outer part of this degraded layer. This is in agreement with observations made by Carde [22].

Between 48 and 61 h of leaching (Fig. 4), phenomena are similar to those already noticed after 24 h of leaching and the thickness of the degraded layer increases. As expected, the degradation front progresses towards the centre of the sample. At 61 h of leaching, the absorption coefficient μ remains constant between 2.3 mm and the surface, meaning that all the Portlandite was dissolved in this part of the sample. The chemical attack leads then to a slower and more progressive decalcification of C-S-H.

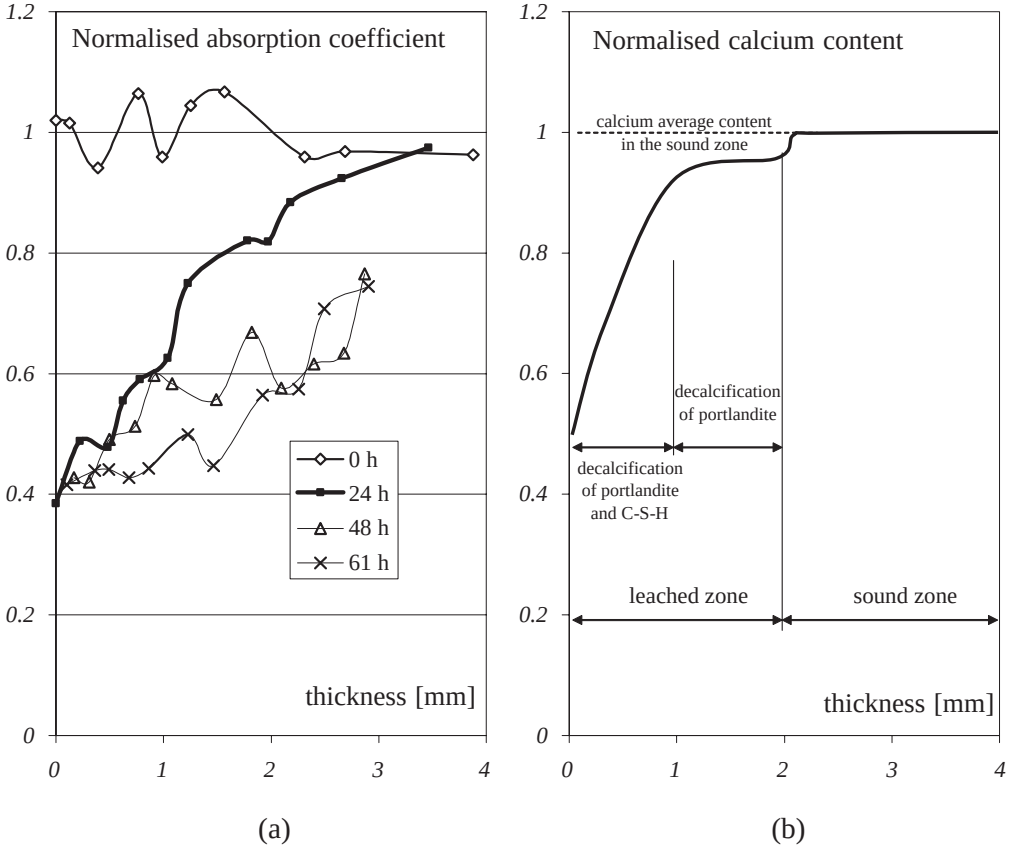

Fig. 10. (a) Normalised absorption coefficient versus thickness in the cement paste; (b) normalized calcium content versus thickness after 24-h leaching, from Refs. [22,31,35].

4.2.2. Leaching front evolution

The position of the leaching front can also be identified by comparing the various degradation stages: we define the first leaching front as the boundary between the sound and the leached zone. Fig. 7 shows cross-sections of the mortar sample numerically reconstructed for the 4 acquisition times: 0, 24, 48 and 61 h of leaching. The distance between these cross-sections to the top of the sample is equal to 5.5 mm: this distance is bigger than the sample radius in order to avoid interference between horizontal and vertical penetrations of the leaching front. In order to have a better accuracy in leaching front measurement, zooms of the complete cross-sections are done and are respectively presented on Fig. 7a, b, c and d. We observe a progressive evolution of the leaching front towards the centre of the specimen (Fig. 7): as expected, after 61 h of leaching, almost complete leaching of the sample has occurred. From these cross-sections, it is possible to find the position of the leaching front with respect to time: this is shown in Fig. 8 where the degraded thickness [millimeters] versus the leaching time [seconds] is plotted. This curve is compared to a classic theoretical solution of diffusion models: the measured kinetics is a square root function of time, which has also been experimentally measured by different authors [19,31]. Both experimental curve and the theoretical one are in good agreement, thus confirming the ability of the microtomography method to measure the leaching front position.

It is also possible to show the evolution of the degradation front in a plane parallel to the main sample axis (Fig. 9). We can note that this front evolves towards the centre of the sample. This section shows that the sample is not totality leached, contrary to the analysis of a cross-section perpendicular to the main sample axis might let thinking. This difference can be attributed to the mortar heterogeneity: if the vertical cross-section had been made according to another direction, the difference would have been less visible.

4.2.3. Validation of X-ray microtomography results

In order to validate the use of this new experimental technique, we compare the obtained results with those given in the literature, in particular the experimental works presented by Carde [22] and Gérard [21]. Fig. 10a shows the profiles of a normalized absorption coefficient according to the thickness, corresponding to the distance measured from the sample surface. This normalized absorption coefficient is equal to the local absorption coefficient, measured by X-ray microtomography in the cement paste, divided by the average absorption coefficient measured on the sound cement. Note that it concerns evolutions only measured in the cement matrix of the mortar and the role of ITZ has to be improved by future works. If we consider that calcium is the main compound undergoing the leaching process, this normalized absorption coefficient may represent the variation of solid calcium content in the sample, measured with regard to the initial calcium content. Fig. 10b shows the variation of the calcium content, normalized by the calcium content in the sound part, versus the thickness for a cement paste attacked for 24 h by an ammonium nitrate solution [22,31,35]. These quantitative data, derived from Carde's work, were obtained by microprobe analysis: we notice qualitative and quantitative good correlations between the variation of the normalized absorption coefficient, measured at 24 h of leaching, and the variation of normalized calcium content, showing the ability of microtomography analysis to measure variation of solid calcium content in a cement paste.

Another way of interpreting the X-rays absorption curves according to the mortar leaching process is to consider that these variations represent an increase in material porosity (see Section 2). In that case, it is possible to define an increase in normalized porosity $\Delta\hat{p}$, corresponding to the effect of the absorption coefficient variation $\Delta\mu(x,y)$, due to material leaching:

$$\Delta\hat{p} = 1 + \frac{\Delta\mu(x,y)}{\bar{\mu}_{\text{sound}}(x,y)} \qquad \text{with}$$

$$\Delta\mu(x,y) = \bar{\mu}_{\text{sound}}(x,y) - \mu(x,y) \tag{7}$$

where $\bar{\mu}_{\text{sound}}(x,y)$ is the mean absorption coefficient measured on the sound sample. If $\Delta\hat{p}=1$, there is no variation of porosity, i.e. the initial porosity is kept constant. For example, $\Delta\hat{p}=2$ corresponds to twice the initial

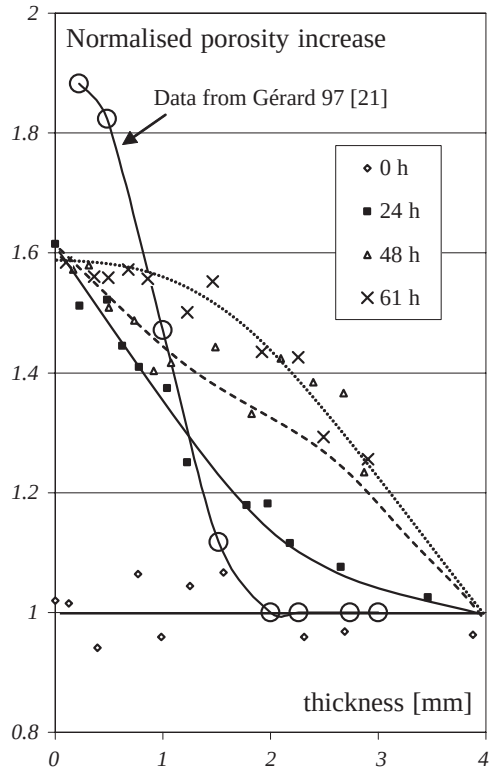

Fig. 11. Comparison between normalised porosity increases measured by microtomography and by SEM image analysis (from Ref. [21]) versus the thickness.

porosity. This increase in porosity corresponds to the calcium dissolution during leaching, by assuming that this dissolution corresponds to creation of a new porosity [21,22]. In Fig. 11, these increases in normalized porosity (for the 4 leaching times) are shown during leaching as a function of the thickness—i.e. the distance from the sample surface, in order to compare this analysis with other experimental results. We notice that the porosity increases from the outside inwards. A comparison is made with the results obtained by Gérard [21], which were obtained by image analysis and SEM observations [36], on a cement paste with 0.55 W/C ratio, leached for 1 month in deionised water. These groups of results are qualitatively comparable: similar changes are found in terms of increase in porosity versus the thickness. Let us note that the difference between the two leaching processes (ammonium nitrate solution and deionised water) lead only to different kinetics: a comparison is then possible as the leaching consequences are the same in both cases [35].

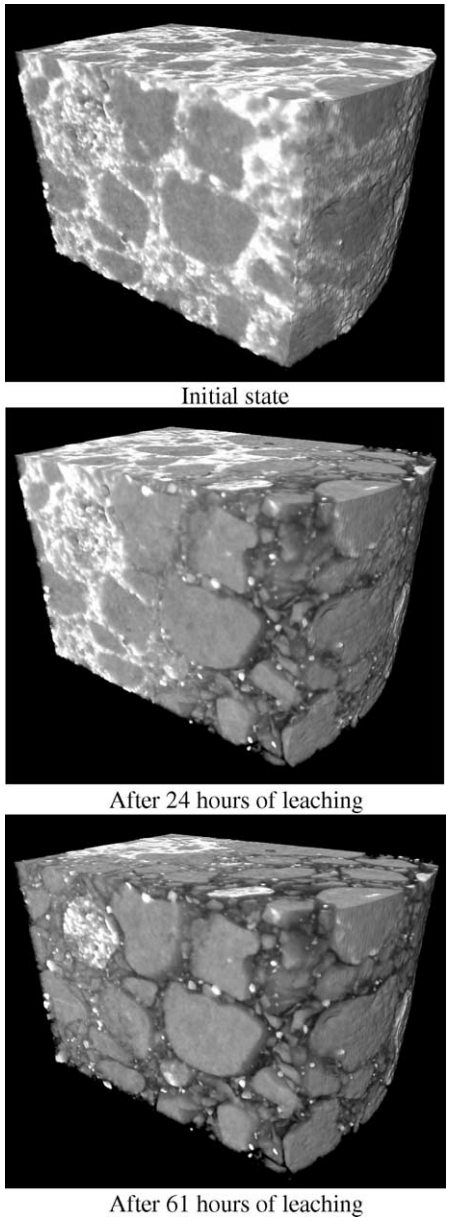

Fig. 12. 3D representation of the same portion of the mortar sample at the different leaching stages. Each data set has been projected on the same system of coordinates after 3D registration giving the possibility to follow precisely the evolution of each voxel individually. Aggregates are in light grey, sound cement in white and leached cement has been set transparent in order to visualise the complex front displacement.

4.3. 3D-reconstructions

An example of a 3D-reconstruction is given Fig. 12, which shows a part of the sample for 3 leaching stage (sound mortar, 24 and 61 h of leaching). It is possible to show aggregates in the degraded zone. The sound cement appears in white at the centre of the sample, the aggregates in light grey. The decrease of X-rays absorption by the leached cement paste occurs as darker on this figure.

The use of this reconstruction allows us to numerically build the pore space and its evolution, in order to obtain quantitative data on the material permeability. A possible use of this digital reconstruction would be to deduce a 3D finite element mesh to allow a mechanical calculation.

5. Conclusions

The synchrotron X-ray computed microtomography is a powerful non-destructive observation technique that finds applications whenever evolution of material microstructure without damage is required. The use of this experimental technique in the field of concrete leaching, as presented here, is new and some preliminary results on the porosity evolution according to the leaching process were described. The XCMT allows us to analyse the mortar microstructure variations in the course of degradation without interaction with the experimental process. Although both the resolution and the sample size are still limited, this technique is very promising for the study of the concrete durability, where the knowledge of the microstructure evolution is of paramount importance in the hope of deriving predictive models.

X-ray computed microtomography allows us to obtain 2D cross-sections and 3D-reconstructions of the mortar microstructure subjected to an accelerated leaching by means of an ammonium nitrate solution. Analysis of the X-ray linear attenuation coefficient variations allows us to quantitatively determine the evolution of the calcium content in solid phase and the increase in porosity, during leaching of a mortar. Additionally, the analysis demonstrated that the siliceous aggregates had no significant role in the leaching process, although an increase in porosity seems to be important in the ITZ. The results show good agreement with literature: the ability of the method to accurately measure the porosity increase of a leached cement paste, without any interaction, was proved. Other studies based on microtomographic analysis are planned as, for example, the

effect of a preliminary drying on mortar leaching kinetics (microcracks induced by drying would increase the reactive surface and the kinetics).

Acknowledgements

We acknowledge the European Synchrotron Radiation Facility for the provision of synchrotron radiation facilities and we would like to thank Peter Cloetens for his assistance in using beamline ID19. Ismail Yurtdas, from the Laboratory of Mechanics of Lille, is acknowledged for his help during the tests. Computations and 3D visualisations have been made possible thanks to the computing equipment partly funded by the Conseil Régional d'Aquitaine.

References

[1] P. Cloetens, R. Barrett, J. Baruchel, J. Guigay, M. Schlenker, Phase objects in synchrotron radiation hard-X-ray imaging, J. Phys., D, Appl. Phys. 29 (1996) 133–146.
[2] J. Baruchel, J.Y. Buffière, E. Maire, P. Merle, G. Peix, X-ray Tomography in Material Science, Hermès Sciences Pub, Paris, 2000.
[3] D. Bernard, G.L. Vignolles, J.-M. Heintz, Synchrotron X-ray micro-tomography: a tool for porous materials evolution modelling, in: J. Baruchel, J.Y. Buffière, E. Maire, P. Merle, G. Peix (Eds.), X-ray Tomography in Materials Science, Hermès Science, Paris, 1999, pp. 177–192.
[4] E.N. Landis, E.N. Nagy, D.T. Keane, Microstructure and fracture in three dimensions, Eng. Fract. Mech. 70 (7–8) (2003) 911–925.
[5] E.N. Landis, E.N. Nagy, Three-dimensional work of fracture for mortar in compression, Eng. Fract. Mech. 65 (2–3) (2000) 223–234.
[6] L.B. Wang, J.D. Frost, G.Z. Voyiadjis, T.P. Harman, Quantification of damage parameters using X-ray tomography images, Mech. Mater. 35 (8) (2003) 777–790.
[7] S.R. Stock, N.K. Naik, A.P. Wilkinson, K.E. Kurtis, X-ray micro-tomography (microCT) of the progression of sulfate attack of cement paste, Cem. Concr. Res. 32 (10) (2002) 1673–1675.
[8] D.P. Bentz, N.S. Martys, P.E. Stutzman, M.S. Levenson, E.J. Garboczi, J. Dunsmuir, L.M. Schwartz, X-ray microtomography of an ASTM C109 mortar exposed to sulfate attack, in: S. Diamond, S. Mindess, F.P. Glasser, L.W. Roberts (Eds.), Microstructure of Cement-Based Systems/Bonding and Interfaces in Cementitious Materials, Materials Research Society, Pittsburgh, 1995, pp. 77–82.
[9] J. Hu, P. Stroeven, X-ray absorption study of drying cement paste and mortar, Cem. Concr. Res. 33 (3) (2003) 397–403.
[10] D.P. Bentz, K.K. Hansen, H.D. Madsen, F. Vallee, E.J. Griesel, Drying/hydration in cement pastes during curing, Mater. Struct. 34 (2001) 557–565.
[11] J. Chotard, M.P. Boncoeur-Martel, A. Smith, J.P. Dupuy, C. Gault, Application of X-ray computed tomography to characterise the early hydration of calcium aluminate cement, Cem. Concr. Compos. 25 (1) (2003) 145–152.
[12] E.J. Garboczi, Three-dimensional mathematical analysis of particle shape using X-ray tomography and spherical harmonics: application to aggregates used in concrete, Cem. Concr. Res. 32 (10) (2002) 1621–1638.
[13] D.P. Bentz, D.A. Quenard, H.M. Kunzel, J. Baruchel, F. Peyrin, N.S. Martys, E.J. Garboczi, Microstructure and transport properties of porous building materials: Part 2. Three-dimensional X-ray tomographic studies, Mater. Struct. 33 (2000) 147–153.
[14] F. Adenot, Durabilité du béton: caractérisation et modélisation des processus physiques et chimiques de dégradation du ciment, Phd Thesis of University of Orléans, France (in French), 1992.
[15] P. Faucon, P. Le Bescop, F. Adenot, P. Bonville, J.F. Jacquinot, F. Pineau, B. Felix, Leaching of cement: study of the surface layer, Cem. Concr. Res. 26 (1996), 1707–1715.
[16] B. Bourdette, Durabilité des mortiers. Prise en compte des auréoles de transition dans la caractérisation et la modélisation des processus physiques et chimiques d'altération, Phd Thesis of INSA de Toulouse, France (in French) 1994.
[17] C. Carde, R. François, Effect of ITZ leaching on durability of cement based materials, Cem. Concr. Res. 27 (1997) 971–978.
[18] A. Delagrave, M. Pigeon, J. Marchand, E. Revertegat, Influence of chloride ions and pH level on the durability of high performance cement pastes, Cem. Concr. Res. 26 (1996) 749–760.
[19] C. Tognazzi, Couplages fissuration/dégradation chimique dans les matériaux cimentaires: caractérisation et modélisations, Phd Thesis of INSA de Toulouse, France (in French), 1998.
[20] E. Revertegat, C. Richet, P. Gegout, Effect of pH on the durability of cement pastes, Cem. Concr. Res. 22 (1992) 259–272.
[21] B. Gérard, Contribution des couplages mécanique-chimie-transfert dans la tenue à long terme des ouvrages de stockage de déchets radioactifs, Phd Thesis of Ecole Normale Supérieure de Cachan, France (in French), 1996.
[22] C. Carde, Caractérisation et modélisation de l'altération des propriétés mécaniques due à la lixiviation des matériaux cimentaires, Phd Thesis of INSA de Toulouse, France (in French), 1996.
[23] D. Bentz, E. Garboczi, Modelling the leaching of calcium hydroxide from cement paste: effects on pore space percolation and diffusivity, Mater. Struct. 25 (1992) 523–533.
[24] F.H. Heukamp, F.-J. Ulm, J. Germaine, Mechanical properties of calcium-leached cement pastes—triaxial stress states and the influence of the pore pressures, Cem. Concr. Res. 31 (2001) 767–774.
[25] C. Le Bellego, B. Gérard, G. Pijaudier-Cabot, Chemo-mechanical effects in mortar beams subjected to water hydrolysis, J. Eng. Mech. -ASCE 126 3 (2000) 266–272.
[26] C. Le Bellégo, Couplages chimie-mécanique dans les structures en béton attaquées par l'eau: étude expérimentale et analyse numérique, Phd Thesis of Ecole Normale Supérieure de Cachan, France (in French), 2001.
[27] C. Tognazzi, O. Didry, M. Carcasses, J.-P. Ollivier, F. Adenot, J.-M. Torrenti, Expériences de dégradation et de diffusion, in: J.-M. Torrenti, O. Didry, J.-P. Ollivier, F. Plas (Eds.), La Dégradation des Bétons, Hermès Science, Paris, 1999, pp. 121–140 (in French).
[28] F.-J. Ulm, J.-M. Torrenti, F. Adenot, Chemoporoplasticity of calcium leaching in concrete, J. Eng. Mech.-ASCE 125 (10) (1999) 1200–1211.
[29] G. Pijaudier-Cabot, B. Gérard, N. Burlion, L. Molez, Localisation of damage in quasi-brittle materials and influence of chemically activated damage, in: R. de Borst, E. van der Giessen (Eds.), Material Instabilities in Solids, John Wiley Sons Ltd, Chichester, England, 1998, pp. 441–456.
[30] F. Bangert, S. Grasberger, D. Kuhl, G. Meschke, Environmentally induced deterioration of concrete: physical motivation and numerical modelling, Eng. Fract. Mech. 70 (7–8) (2003) 891–910.
[31] C. Carde, R. François, J.-M. Torrenti, Leaching both calcium hydroxyde and C-S-H from cement paste: modeling the mechanical behaviour, Cem. Concr. Res. 26 (1996) 1257–1268.
[32] J.M. Torrenti, F. Adenot, C. Tognazzi, S. Danese, S. Poyet, Application du modèle de dégradation du béton au cas des milieux fissurés et au couplage avec la mécanique, Sciences des matériaux et propriétés des bétons, 1ères rencontres internationalesToulouse, France, March 5–6 1998, 1998 (in French).
[33] D. Bernard, D. Gendron, J.-M. Heintz, S. Bordere, J. Etourneau, First direct 3D visualisation of micro structural evolutions during sintering through X-ray computed microtomography, Acta Mater. 53 (2005) 121–128.

[34] M. Mainguy, F.-J. Ulm, F.H. Heukamp, Similarity properties of demineralization and degradation of cracked porous materials, Int. J. Sol. Struct. 38 (2001) 7079–7100.
[35] C. Carde, R. François, Effect of the leaching of calcium hydroxide from cement paste: modeling on mechanical and physical properties, Cem. Concr. Res. 27 (1997) 539–550.
[36] A. Ammouche, Caractérisation automatique de la micro fissuration des bétons par traitement d'images. Application à l'étude de différents faciès de dégradation, Phd thesis Université Bordeaux 1 (France)/ Université Laval (Canada) (in French), 1999.